IEEE Access
Multidisciplinary | Rapid Review | Open Access Journal

Received 5 March 2023, accepted 25 April 2023, date of publication 2 May 2023, date of current version 10 May 2023.

Digital Object Identifier 10.1109/ACCESS.2023.3272482

RESEARCH ARTICLE

DeepCurvMRI: Deep Convolutional Curvelet Transform-Based MRI Approach for Early Detection of Alzheimer's Disease

CHAHD M. CHABIB[1], LEONTIOS J. HADJILEONTIADIS[1,2], (Senior Member, IEEE), AND AAMNA AL SHEHHI[1]

[1]Department of Biomedical Engineering, Khalifa University, Abu Dhabi, United Arab Emirates
[2]Department of Electrical and Computer Engineering, Aristotle University of Thessaloniki, 54124 Thessaloniki, Greece

Corresponding author: Aamna Al Shehhi (aamna.alshehhi@ku.ac.ae)

This work was supported by Khalifa University.

ABSTRACT Alzheimer's Disease (AD) is the most common form of dementia. It usually manifests through progressive loss of cognitive function and memory, subsequently impairing the person's ability to live without assistance and causing a tremendous impact on the affected individuals and society. Currently, AD diagnosis relies on cognitive tests, blood tests, behavior assessments, brain imaging, and medical history analysis. However, these procedures are subjective and inconsistent, making an accurate prediction for the early stages of AD difficult. This paper introduces a curvelet transform (CT) based-convolutional neural network (CNN) (DeepCurvMRI) model for improving the accuracy of early-stage AD disease detection using from Magnetic resonance imaging (MRI) images. The MRI images were first pre-processed using CT, and then a CNN model was trained using the new image representation. In this study, we used Alzheimer's MRI images dataset hosted on the Kaggle platform to train DeepCurvMRI for multi and binary classification tasks. DeepCurvMRI achieved an accuracy, sensitivity, specificity, and F1 score of 98.62% $\pm$ 0.10%, 99.05% $\pm$ 0.10%, 98.50% $\pm$ 0.03%, and 99.21 $\pm$ 0.08, respectively, using the leave-one-group-out (LOGO) cross-validation approach in multi-classification task. The highest accuracy obtained in binary classification is 98.71% $\pm$ 0.05%. In addition to LOGO, DeepCurvMRI was tested using randomly stratified 10-fold and 5-fold cross validation. These encouraging results are superior to the ones reported in related methods, showcasing the potentiality of DeepCurvMRI in capturing the key anatomical changes in MRI images that can be differentiated between various staged of Alzheimer's disease classes.

INDEX TERMS Alzheimer's disease, curvelet transform, deep learning, CNN, MRI images.

I. INTRODUCTION

Alzheimer's disease (AD), the most common type of dementia, is a neurodegenerative disease that deteriorates brain connections, leading to memory impairment and decline in other cognitive functions [1]. In 2018, it was estimated that over 50 million people worldwide were living with dementia, and this number is expected to reach 152 million by 2050 [2]. The average life expectancy after AD diagnosis is 3-9 years [3], as currently, there is no cure for AD, and in the past 20 years, the Food and Drug Administration (FDA) has approved only two types of drugs to treat some symptoms of AD [4]. The stages of AD can be divided into two stages: Mild Cognitive Impairment (MCI), and Alzheimer's disease (AD). The MCI stage can be subdivided further into Early Mild Cognitive Impairment (EMCI) and Late Mild Cognitive Impairment (LMCI). Individuals with MCI face a significant risk in progressing into the late stages of Alzheimer's [5]. MCI patients experience a mild decline in memory and other cognitive functions. At a later stage, the patient would be unable to respond to the environment or carry on a conversation. Therefore, early AD detection would significantly contribute to preventive treatment and help delay cognitive deterioration [6]. Accurate diagnosis of the disease requires

The associate editor coordinating the review of this manuscript and approving it for publication was Marco Giannelli.

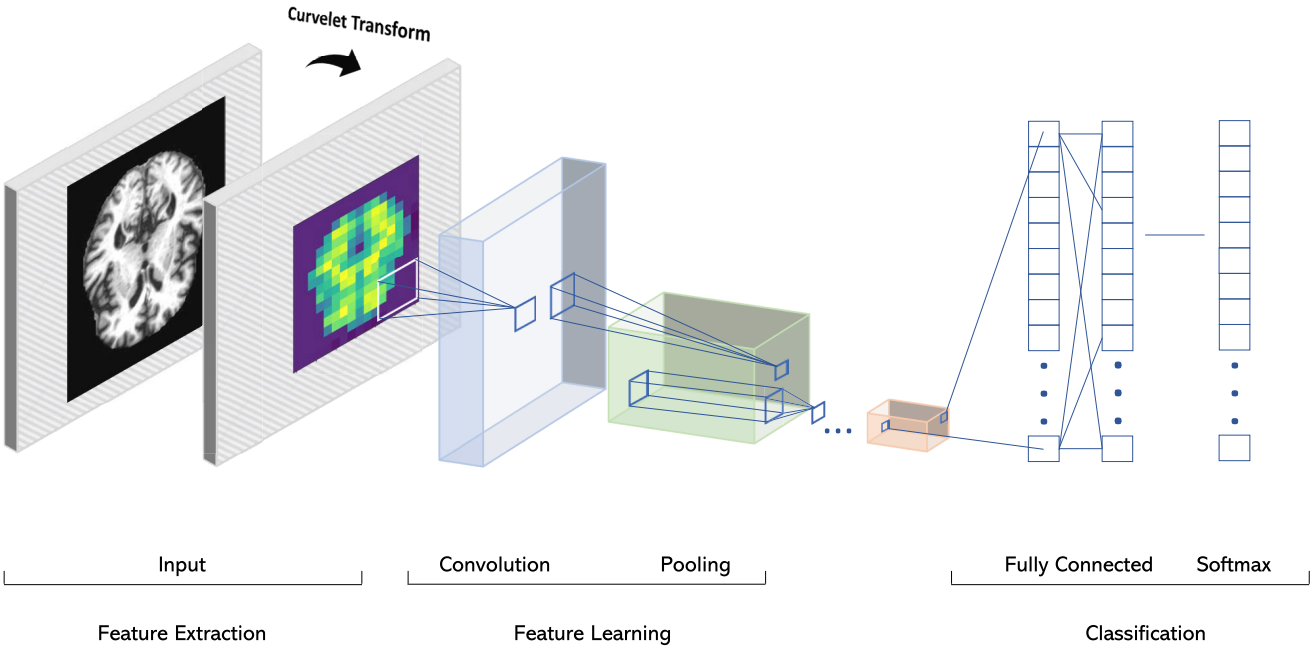

FIGURE 1. DeepCurvMRI model workflow process for classifying Alzheimer's stages using MRI images.

a series of examinations: cognitive tests, blood tests, behavior assessments, brain imaging, and medical history analysis [7], [8], [9]. However, the current examination relies explicitly on behavioral assessments and the patient's medical history as pieces of evidence, which both demand multiple testing sessions by expert doctors over a long period. The latter increases the diagnosis cost and brings subjectivity and alterity to the diagnostic outcome [10]. As a result, a more efficient and cost-effective diagnostic system is crucial. Recently, with the advancement in technology, several imaging techniques have been developed, such as Magnetic Resonance Imaging (MRI) [11], Positron Emission Tomography (PET) [12], and Computed Tomography (CT) [13]. These techniques are non-invasive, rapid, accurate, and are widely used to obtain additional information about AD diagnosis. At the same time, artificial intelligence (AI) has been significantly developed in the recent years and offered substantial advantages in computer-based diagnostic systems [14], [15], [16]. Over the past years, various efficient machine learning (ML) algorithms have been designed to improve disease diagnosis accuracy [17]. Research interests in this domain include both Support Vector Machine (SVM) [18], [19], [20], [21] and Deep Learning (DL) models [22].

SVM and regular neural networks have been criticized for their poor classification performance when trained on the raw/un-preprocessed data [23], [24], [25]. A series of feature preprocessing algorithms combined with the classifier is necessary for improving the classifier accuracy. For example, Kamal et al. [26] preprocessed MRI images using an adaptive mean filter and histogram equalization. Afterwards, image features were extracted using Haar Transform for the binary classification of AD using SVM. Additionally, Wang et al. [27] trained AdaBoost as a classifier for AD diagnosis, while intermediate features were processed and selected from brain gray-matter images using kernel principal component analysis (KPCA). In short, such methods heavily depend on a series of feature processing algorithms to classify improve the ML performance.

In contrast, DL models can take the raw data as input and find discriminating features in the training dataset during model traning, such as Convolutional Neural Networks (CNNs) [28], [29], Recurrent Neural Networks (RNNs) [30], and Multi-Layer Perceptrons (MLP) [31]. CNN models are frequently used to extract features from PET or MRI images for their ability to detect essential attributes accurately and automatically with high-processing speed. MRI images are easier to access than PET as they require less processing time and are less expensive. AlSaeed and Omar [32] utilized ResNet50, a pre-trained CNN model, to automatically extract AD diagnosis features using MRI images. They obtained an accuracy ranging from 73 to 99%. Hogan and Christoforou [33] developed a 3D CNN model to identify biological markers of AD from MRI images, giving an accuracy of 80% on the testing dataset. Moreover, it has been proven that a feature extraction approach in combination with CNN classification can improve the final prediction result and decrease the training time compared to ML approach [34], [35], [36], [37].

Recently, Anitha et al. [38] proposed a WT-CNN model for AD image classification, in which wavelet transform

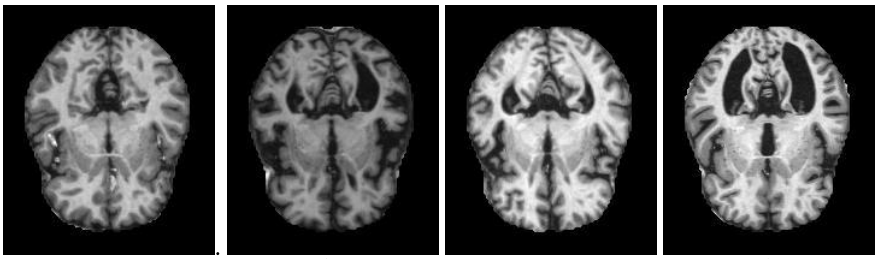

FIGURE 2. Examples of brain MRI images from four different classes, i.e.: (a) ND, (b) VMD, (c) MID, and (d) MOD.

(WT) is applied as a feature extraction method prior to training the CNN model. WT-CNN model achieved an accuracy of 91.87%, which is 1.63% higher than the CNN model. WT can detect features overlooked by other feature extraction methods, such as breakdown points and discontinuities. Several other studies have also utilized WT as a tool for feature extraction in the form of wavelet coefficients from MRI images [26], [39], [40], [41]. However, WT's major limitation is its inability to identify curved edges, which in some cases causes false alarms. A more advanced approach is utilizing Curvelet Transform (CT) as a feature extraction method for its ability to obtain both linear and curved edges along multiple scales and orientations [42]. In this regard, several studies have applied CT in various computer vision tasks, namely tumor detection [43], [44], image segmentation [45], [46], [47], signature verification [48], [49], and face recognition [50], [51], [52]. However, despite its advantages, limited number of studies have reported using CT as a feature extraction tool for AD detection using MRI images [53], [54].

In this article, we propose a novel CT-based CNN model named DeepCurvMRI that improves AD stage prediction accuracy using MRI images. The model incorporates Fast Discrete CT (FDCT) for feature extraction across multiple scales and orientations. Followed by a shallow CNN network for the multi-class classification (Non-Demented (ND) vs. Very Mild Demented (VMD) vs. Mild Demented (MID) vs. Moderate Demented(MOD)) and binary classification(ND vs. VMD). The major contributions of the paper are summarized as follows:

- A novel Curvelet Transform-based Convolutional Neural Network approach is proposed, which provides a more effective and faster method for AD diagnosis.
- Fast Discrete Curvelet Transform is applied as a feature extraction tool for AD MRI image classification for the first time.
- In comparison with other models, DeepCurvMRI requires less number of training parameters, giving a high classification accuracy in a short period.
- DeepCurvMRI shows better accuracy in comparison to VGG-16 and AlexNet.

The rest of the paper are organized as follows. Section II provides details of the data used in this research and introduces the proposed DeepCurvMRI approach. Section III evaluates the performance of DeepCurvMRI and discusses the results. Section IV concludes the paper.

TABLE 1. Number of images in the obtained Kaggle dataset.

Class	No. of Images
Non-Demented (ND)	3200
Very Mild Demented (VMD)	2240
Mild Demented (MID)	896
Moderate Demented (MOD)	64

II. THE PROPOSED DeepCurvMRI FRAMEWORK

The overall flow of the DeepCurvMRI is illustrated in Fig. 1. The model consists of three main steps: Data pre-processing, feature extraction using Curvelet Transform, and classification. Each step is discussed below.

A. DATA DESCRIPTION AND PRE-PROCESSING

The AD MRI dataset used here was obtained from the open-source platform Kaggle,[1] which consists of 6400 MRI images of four classes, i.e., Non-Demented (ND), Very Mild Demented (VMD), Mild Demented (MID), and Moderate Demented (MOD). The dataset contains 200 subjects, with 32 horizontal slices of the brain for each subject. To avoid information leakage, the training and testing sets were united, and leave-one-group-out and k-fold cross validation were performed. The original image size is 176×208. All images were resized into 208×208. Fig. 2 shows the typical brain MRI samples for each class. Table 1 provides dataset distribution with a number of images in the obtained dataset.

B. FEATURE EXTRACTION USING FAST DISCRETE CURVELET TRANSFORM

Curvelet is an excellent Multiscale Geometric Analysis (MGA) approach. CT reserves the same decomposition benefits reported with the WT, but has the additional advantage of compact representation of edges and singularities on curves along multiple scales and directions [42], [55]. As a matter of fact, CT is commonly used to obtain sparse representations of

[1] https://www.kaggle.com/datasets/tourist55/alzheimers-dataset-4-class-of-images

smooth objects with discontinuity along curves. In this work, Fast Discrete Curvelet Transform (FDCT) is applied to AD MRI images to detect low-level features and reduce roughness and noise-amplifications within the decomposed images. This allows the detection of local and regional differences in brain images between AD and control subjects. The input to FDCT is Cartesian arrays $f[x_1, x_2]$ (representing an image), where $0 < x_1, x_2 < n$. This results in a collection of curvelet coefficients generated by 2D Fourier plane, as indicated in equation 1, in which $\Phi_{j,l,k}$ denotes the curvelet basis function indexed by orientation l, scale j, and spatial positions (k_1, k_2).

$$\Phi_{j,l,k_1,k_2} = \sum f(x_1, x_2)\Phi^d_{j,l,k_1,k_2}[x_1, x_2] \tag{1}$$

$\Phi^d_{j,l,k}$ denotes the digital curvelet waveforms.

In the theory of CT, two main approaches can be used to obtain the curvelet coefficients, namely Unequal Space Fast Fourier Transform (USFFT) method and Wrapping-based method [55]. USFFT generates the coefficients by sampling the Fourier image samples in an irregular manner, making the frequency curvelet response appear to be a trapezoidal wedge. Furtherly, all scales and orientational coefficients are generated in an ascending order. With the Wrapping-based method, on the other hand, the wedge is wrapped into a rectangle shape to perform the inverse Fourier transform. The wrapping is applied via periodic tiling of the spectrum using the rectangular wedge to collect the coefficients. Both Wrapping-based and USFFT methods produce identical results. However, the Wrapping-based method is applied here, as it is more time efficient and requires less computational resources in comparison than USFFT. Fig. 3 illustrates the curvelet wrapping architecture. If $\hat{f}[x_1, x_2]$ denotes the Cartesian arrays' 2D discrete Fourier transform, then the construction of the FDCT via wrapping is as follows:

1) Apply 2D Fast Fourier Transform to generate Fourier samples

$$\hat{f}[x_1, x_2], \quad -\frac{x}{2} \leq x_1,\ x_2 < \frac{x}{2} \tag{2}$$

2) If $\hat{U}[x_1, x_2]$ is the discrete localizing window, then form the product for each scale (j) and orientation (l)

$$\hat{U}_{j,l}[x_1, x_2]\hat{f}[x_1, x_2] \tag{3}$$

3) Wrap the product around the origin to obtain

$$\tilde{f}_{j,l}[x_1, x_2] = W(\hat{U}_{j,l}\hat{f})[x_1, x_2] \tag{4}$$

where the ranges for x_1 and x_2 are $0 \leq x_1 < 2^j$ and $0 \leq x_2 < 2^{j/2}$, respectively.

4) Apply the inverse 2D Fast Fourier Transform to all $\tilde{f}_{j,l}$ in order to obtain the discrete curvelet coefficients Φ_{j,l,k_1,k_2}

The number of scales represents resolution, which depends on the size of the original image. The maximum image size in the dataset is 176×208 pixels; thus, the maximum number of scales to be used is 5. Scales 1 and 5, scale 2, and

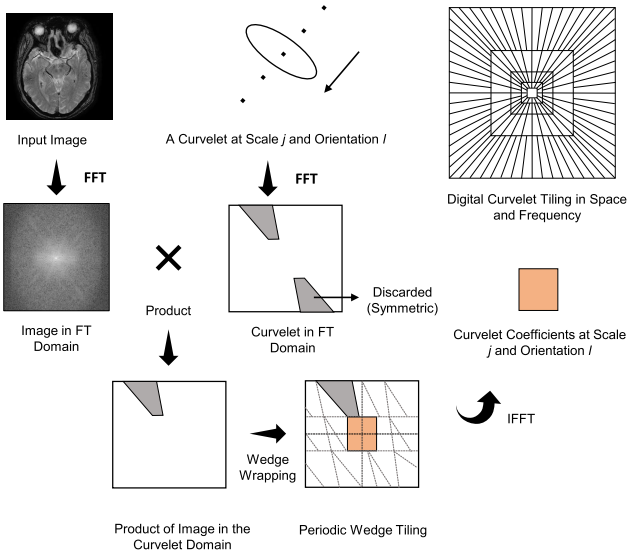

FIGURE 3. FDCT via wrapping.

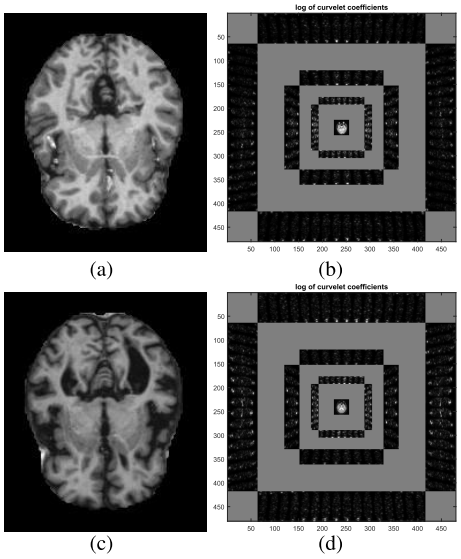

FIGURE 4. Example of MRI images and their FCT: (a) ND brain, (b) decomposed curvelet sub-bands of (a), (c) VMD brain, and (d) decomposed curvelet sub-bands of (c).

scales 3 and 4 contain 1, 16, and 32 orientations, respectively, giving a total of 82 subbands. Figure 4 illustrates the decomposed images for an ND brain (Fig. 4(a)) and VMD brain (Fig. 4(c)). The Cartesian concentric coronae are characterized by the course level, the dyadic spatial square, and the fine levels surrounding the center, representing higher frequencies. The selection of specific scales and orientations is essential to avoid redundancy in information. The first scale of MRI images in the curvelet domain corresponds to the general information in the images. As, the scale increases, the noise content increases. Hence, for this type of image, it is sufficient to utilize the coarse scale, as the original image resolution is low. Thus, increasing scales does not necessarily lead to improvements in the classification accuracy.

C. CURVELET DOMAIN DENOSING USING KURTOSIS

Due to its multiscale and multidirectional advantages, CT is an effective tool for extracting meaningful information and suppressing noise in seismic data [56], [57]. Before applying deep learning, it is necessary to remove coefficients associated with noise by setting a proper threshold. Signals produced by curvelet transform are normally found in lower scales and specific orientations, while noise can be distributed over all scales and directions. As the scale increases, the noise present within the curvelet matrices increases. Thus, curvelet coefficients can be processed with a scale-dependent threshold as the following:

$$\hat{\Phi}_{(j,l,k)} = \begin{cases} 0, & |\Phi_{j,l,k_1,k_2}| < Thr_j \\ \Phi_{(j,l,k)}, & \text{else} \end{cases} \quad (5)$$

where $\hat{\Phi}_{(j,l,k)}$ is the thresholded curvelet coefficients and Thr_j is the threshold value. In the curvelet domain denoising, a crucial step is to estimate a threshold from the curvelet noisy coefficients. Donoho and Johnstone [58] proposed a multi-scale threshold value (Thrj) as

$$Thr_j = \alpha\sqrt{2log(N)} \times 2^{-(J-j)/2}, \quad j = 1, 2, \ldots, J \quad (6)$$

where is the standard deviation, N is the total number of coefficients, and J denotes the total number of decomposition scales. Lin et al. [59] improved on the above threshold value and proposed incorporating kurtosis statistics. Kurtosis is a measure of non-Gaussian characteristic for a random variable. Noise is generically non-Gaussian in nature. In image processing, noise found in images can be highly non-Gaussian. Thus, one possible way to remove noisy coefficients is by thresholding based on kurtosis. A high kurtosis value indicates the presence of coefficients that carry crucial information, while a low kurtosis value indicates noise. Weighting the multi-scale threshold according to the coefficients kurtosis matrix gives

$$\text{Thr}_j = \alpha\sqrt{2log(N)} \times 2^{-(J-j)/2}(1 - |\frac{K(k)}{K_{max}(k)}|), \quad j = 1, 2, \ldots, J \quad (7)$$

where $K(k)$ is the kurtosis of the curvelet coefficients calculated over a sample block, and $K_{max}(k)$ is the maximum kurtosis found among all sample blocks [59]. Kurtosis is calculated over a sample block using the following equation:

$$K(k) = \frac{E[(x-\mu)^4]}{\xi^4} \quad (8)$$

x denotes a curvelet coefficient, E is the expectation, μ is the mean, and ξ is the standard deviation. A sliding window with a size of (3,3) is applied in this work. Fig. 5 represents the reconstructed curvelet coefficients of an AD MRI image in the coarse scale before and after kurtosis threshholding.

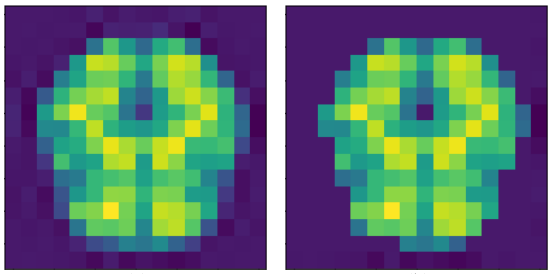

FIGURE 5. Reconstructed curvelet coefficients of an AD MRI image in the coarse scale (a) before kurtosis thresholding, and (b) after kurtosis thresholding.

TABLE 2. DeepCurvMRI architecture details.

Layer Type	Output Shape	Parameters
Conv2D + ReLU	(None, 12, 12, 50)	1850
BatchNormalization	(None, 12, 12, 50)	200
MaxPooling2D	(None, 6, 6, 50)	0
Conv2D_2 + ReLU	(None, 1, 1, 25)	45025
BatchNormalization_2	(None, 1, 1, 25)	100
MaxPooling2D_2	(None, 1, 1, 25)	0
Dropout	(None, 1, 1, 25)	0
GlobalAveragePooling2D	(None, 25)	0
Dense	(None, 160)	4160
Softmax layer	(None, 4)	644

D. CLASSIFICATION USING CONVOLUTIONAL NEURAL NETWORKS

After feature extraction with Curvelet Transform, specific angles and subbands are fed into a CNN model to determine the areas most affected by Alzheimer's within the MRI images. To classify Alzheimer's stages, the CNN model is built from scratch. The proposed model consists of two convolutional layers with Rectified Linear Unit (ReLU) activation function, two batch normalization layers, two max-pooling layer, a global average pooling layer, a dropout layer, a dense layer, and a Softmax classification layer. Fig. 6 illustrates the architecture of the DeepCurvMRI model. Tabl. 2 represents DeepCurvMRI architecture details. The DeepCurvMRI parameters are represented in Table 3.

1) INPUT LAYER

The input layer is the first layer in the DeepCurvMRI model, where threshholded curvelet matrices at scale 1 for all images are given as an input. The threshholded curvelet matrices at the coarse scale have a size of 17×17, thus making the input image size 17×17.

2) CONVOLUTIONAL LAYERS

Conventional layers are the primary building block of the DeepCurvMRI model. They receive an image as an input and convolve using filters to produce an output image. The output at each channel is known as a feature response or map, and it

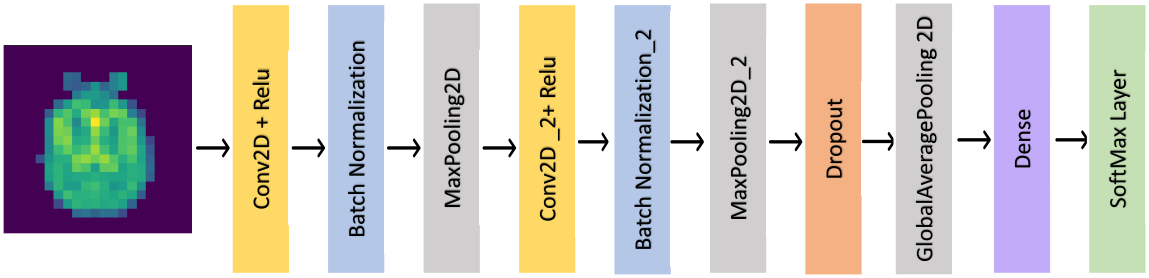

FIGURE 6. Architecture of DeepCurvMRI model for the multi-class classification of Alzheimer's disease stages.

TABLE 3. Significant parameters of the DeepCurvMRI model.

Parameter	Value
Input Channels	3
Batch Size	35
Stride	1 x 1
Number of Filters	50,25
Filter Size	6 x 6
Pool Size	2 x 2
Learning Rate	0.0001
Activation Function	ReLU
Optimizer	Adam

is calculated as follows:

$$x_n = I \times W_n + B_n, \quad n = 1, 2, \ldots, F \tag{9}$$

where I is the input, x_n is the output of the nth filter, W_n is the weight of the nth filter, B_n is the bias of the nth filter, and F is the number of filters. In the DeepCurvMRI model, the number of filters for the first and second convolution are 9 and 12, respectively, and both have a filter size of 3×3 (see Table 2). In this work, the ReLU activation function has been applied directly to the feature map output.

3) BATCH NORMALIZATION LAYERS

Batch normalization layers are used after conventional layers to reduce the effect of initialization and speed up the process of training by recenting and rescaling. Batch normalization applies a transformation that keeps the output standard deviation close to 1 and the mean output close to 0. The values are normalized according to the following equation:

$$y_i = \alpha \hat{x_i} + \beta \tag{10}$$

in which y_i represents the output values, $\hat{x_i}$ the normalized input values, α the scale, and β the offset factor.

4) POOLING LAYERS

Pooling layers are applied after convolution layers to reduce the size of the feature map, thus decreasing the number of parameters required and lower computational cost. Max-pooling layers pick maximum pixel values in the filter map selected by the kernel filter. The result is a feature map containing the most prominent features of the convolutional layer's outputted feature map. Maximum pooling is computed with the following equation

$$MP = Floor\left(\frac{X - F}{s} + 1\right) \tag{11}$$

where X is the input, F is the max-pooling window size, s is stride. After max pooling, a global average pool (GAP) is applied to reduce the dimensions of the feature map and produce a 2D feature vector. Unlike a flatten layer, GAP considers the spatial information, making it more robust to spatial translations of the input.

TABLE 4. Performance of DeepCurvnMRI with three validation approaches(i.e. LOGO, 10-Fold, and 5-Fold).

Classification	Approach	Acc%	Sens%	Specs%	F1 score
Binary (ND/VMD)	LOGO	98.71 ±0.05	98.84±0.03	98.50 ±0.03	99.25 ±0.01
	5-Fold	97.41 ±0.04	97.80±0.03	98.01 ±0.04	98.20 ±0.03
	10-Fold	97.61 ±0.06	97.85±0.04	97.90 ±0.04	98.10 ±0.05
Multiclass	LOGO	98.62 ±0.10	99.05 ±0.10	98.5 ±0.10	99.21 ±0.08
	5-Fold	97.83±0.03	97.80 ±0.03	98.10 ±0.02	98.70 ±0.05
	10-Fold	97.62±0.03	97.50 ±0.01	98.00 ±0.02	98.50 ±0.04

5) DROPOUT LAYER

Dropout is performed to randomly drop a fraction of the neurons in the GAB layer to avoid some variables from being repeatedly accepted during the training. This layer also aids in reducing over-fitting. The dropout value applied here is 0.5.

6) DENSE LAYER

The fully connected or dense layer is a standard feedforward layered network that includes input neurons, hidden neurons, and a softmax regression unit. The output of the GAP layer is fed to the dense layer. In the proposed method, 64 neurons are used in the dense layer, after which a softmax layer is applied to classify the classes. The softmax layer generates the probability distribution of the classification results for each pixel.

E. MODEL EVALUATION

Due to the limited number of patients in the dataset, DeepCurvMRI performance was assessed using two different methods: leave-one-group-out cross-validation (LOGOCV)

TABLE 5. Performance analysis of DeepCurvnMRI with different models.

Method	Classifier	Classification	Dataset	Acc. (%)	F1 Score (%)	Number of parameters	Reference
Neural Network	VGG-16	Binary	Kaggle	70.30	52.0	138,627,867	[60]
Neural Network	SVM	Binary	Kaggle	73.0	-	-	[61]
Neural Network	Feed-forward LPQNet	Binary	Kaggle	99.64	- -	[62]	
Neural Network	HTLML	Multi-class	Kaggle	91.75	90.25	-	[63]
Neural Network	AlexNet	Multi-class	Kaggle	94.0	94.12	60,000,000	[64]
Neural Network	DEMENT	Multi-class	Kaggle	95.23	95.27	4,534,996	[65]
FDCT-WR	CNN	Binary (ND vs. VMD)	Kaggle	98.71	99.25	43,721	DeepCurvMRI
FDCT-WR	CNN	Multiclass	Kaggle	98.62	99.21	51,797	DeepCurvMRI

FDCT-WR: Fast Discrete Curvelet Transform - Wrapping Method.

and stratified k-fold cross validation. LOGOCV involves using $N_g - 1$ groups ($N_s = 200$) as training sets and one group as a test set for validation. This process is repeated N_g times until each group has been used as the test set. On the other hand, stratified k-fold cross validation randomly selects a fraction of the data $\frac{1}{k}$ x 100% for testing purposes and uses the remaining data for training. The classification model is reinitialized in each iteration and the subjects from the previous iteration are included in the training. This process is repeated for k iterations. To assure the robustness of the developed model, we performed the randomly stratified k-fold cross validation approach with two values of k, i.e. 10 and 5. We evaluated the performance of DeepCurvMRI using the following metrics: Accuracy, F1-score (F1), Specificity, and Sensitivity.

$$Accuracy = \frac{TP + TN}{TP + TN + FP + FN} \tag{12}$$

$$F1score = \frac{2TP}{2TP + FP + FN} \tag{13}$$

$$Specificty = \frac{TN}{TN + FP} \tag{14}$$

$$Sensitivty = \frac{TP}{TP + FN} \tag{15}$$

where TP is the number of correctly classified Alzheimer's disease subjects; TN is the number of correctly classified non-demented subjects; FP is the number of non-demented and intermediate subjects classified as Alzheimer's disease; and FN is the number of Alzheimer's disease and intermediate subjects classified as non-demented.

III. EXPERIMENTAL RESULTS AND DISCUSSION

A. EXPERIMENTATION RESULTS OF THE PROPOSED DeepCurvMRI MODEL

This subsection presents the experimental results of the proposed DeepCurvMRI model for the multiclass and binary classification of AD. Adam optimizer was utilized with a learning rate of 10^{-3}. The diagnostic abilities of the proposed DeepCurvMRI were evaluated on the aforementioned 200 subjects (see section II) that have been included in this study using a leave-one-group-out (LOGO) cross-validation approach and different k-fold approaches (5-fold and 10-fold). We evaluated the performance of our model using overall accuracy, sensitivity, specificity, and F1-score. The classification process has outputted the results tabulated in Table 4 in terms of the adopted performance metrics. With accuracy, sensitivity, specificity, and F1 score of 98.62% ± 0.10%, 99.05%±0.10%, 98.50%±0.03%, and 99.21±0.08, respectively, for the LOGOCV, 97.62% ± 0.03%, 98.00% ± 0.02%, and 98.50 ± 0.04, respectively, for the 10-fold, and 97.83% ± 0.03%, 97.80% ± 0.03%, 98.10 ± 0.02, and 98.70 ± 0.05, respectively, for the 5-fold, DeepCurvMRI proves itself as the best among common deep learning models. The highest accuracy, sensitivity, specificity, and F1 score achieved in binary classification is 98.71% ± 0.05%, 98.84%±0.03%, 98.50%±0.03%, and 99.25±0.01, respectively, using LOGOCV. Table 5 summarizes the comparison results between the performances of different DL models and approaches. These results indicate that incorporating image transformation as a feature extraction method with a deep learning model can drastically improve accuracy and lower training duration.

B. DISCUSSION AND COMPARISON

This research aims to provide a detection system for Alzheimer's Disease stages using MRI images to improve the diagnostic accuracy in medical centers. The first step in the proposed model is applying curvelet transformation as a feature extraction function on the collected images. The next step is implementing kurtosis thresholding to remove curvelet coefficients associated with noise. Afterward, the images were reconstructed from the thresholded curvelet coefficients and were classified using CNN classifier. Results in Tabl. 5 express curvelet transformation's ability to capture the key anatomical changes in the brain MRI images, which can be utilized to differentiate between the ND, VMD, MID, and MOD classes. By feeding the deep learning network the output from the FCT, a new space of the MRI representation is created, giving a high classification accuracy.

Table 5 compares the performance analysis of DeepCurvMRI with other models. The existing methods were trained on the binary and multi-class classification on same dataset utilized in this article. DeepCurvMRI is compared to models such as VGG-16 [60], AlexNet [64], DEMENT [65], SVM [61], HTLML [63], and Feed-forward LPQNet [62]. LPQNET achieved slightly higher accuracy than

DeepCurvMRI for the binary classification of AD. However, cross-validation has yet to be applied in LPQNet to account for leakage possibility within the Kaggle Dataset, as there are 32 MRI slices for each patient. DeepCurvMRI outperforms all the other models in terms of accuracy and F1-score, as evidenced by the results of classifying four classes with 51,797 parameters. The performance of DeepCurvMRI is 28.41% higher than VGG-16 and 4.62% higher than AlexNet. Both models utilize millions of parameters. This is attributed to curvelet transformation and its ability to represent smooth objects with discontinuities along curves. A better image representation yields significantly better results within a shorter period. Moreover, thresholding curvelet coefficients using kurtosis removes coefficients associated with noise, providing a more precise representation of the MRI images. Within the Kaggle dataset, a 0.35% increase in accuracy is observed for the multiclass classification of AD. Kurtosis thresholding can be more advantageous based on the clarity of the input images.

IV. CONCLUSION

This work proposes a curvelet-based CNN structure for the binary classification of AD MRI images. DeepCurvMRI is trained and tested using the Kaggle database to classify Alzheimer's disease stages. FCT with wrapping method is used to decompose the MRI image into scales and sub-bands. The obtained curvelet coefficients are then processed and thresholded using kurtosis to extract prominent features. Our model achieved an overall accuracy, sensitivity, specificity, and F1 score of $98.62\% \pm 0.10\%$, $99.05\% \pm 0.10\%$, $98.50\% \pm 0.03\%$, and 99.21 ± 0.08, respectively, using LOGOCV for the multiclass classification of AD, and an accuracy, sensitivity, specificity, and F1 score of $98.71\% \pm 0.05\%$, $98.84\% \pm 0.03\%$, $98.50\% \pm 0.03\%$, and 99.25 ± 0.01, respectively, for the binary classification of ND/VMD. DeepCurvMRI surpassed the performance of the existing methods. Hence, the results showcase the potentiality of the proposed DeepCurvMRI to efficiently identify brain regions associated with AD MRI images, serving as a fast and easy to implement the tool for assisting physicians in AD diagnosis. As for future work, DeepCurvMRI will be trained and tested on various datasets for Alzheimer's disease diagnosis. Moreover, metadata such as clinical biomarkers and demographics can be included and combined to create a holistic approach to AD diagnosis.

REFERENCES

[1] M. Goedert and M. G. Spillantini, "A century of Alzheimer's disease," *Science*, vol. 314, no. 5800, pp. 777–781, 2006. [Online]. Available: https://www.ncbi.nlm.nih.gov/pubmed/17082447

[2] World Health Organization. (Sep. 2021). *Dementia*. [Online]. Available: https://www.who.int/news-room/fact-sheets/detail/dementia

[3] L. L. Barclay, A. Zemcov, J. P. Blass, and J. Sansone, "Survival in Alzheimer's disease and vascular dementias," *Neurology*, vol. 35, no. 6, p. 834, 1985.

[4] M. N. Sabbagh, S. Hendrix, and J. E. Harrison, "FDA position statement 'early Alzheimer's disease: Developing drugs for treatment, guidance for industry,'" *Alzheimer's Dementia, Transl. Res. Clin. Intervent.*, vol. 5, no. 1, pp. 13–19, Jan. 2019.

[5] R. Petersen, "Early diagnosis of Alzheimers disease: Is MCI too late?" *Current Alzheimer Res.*, vol. 6, no. 4, pp. 324–330, Aug. 2009.

[6] National Institute on Aging. (Jul. 2021). *Alzheimer's Disease Fact Sheet*. [Online]. Available: https://www.nia.nih.gov/health/alzheimers-disease-fact-sheet

[7] F. Bature, B.-A. Guinn, D. Pang, and Y. Pappas, "Signs and symptoms preceding the diagnosis of Alzheimer's disease: A systematic scoping review of literature from 1937 to 2016," *BMJ Open*, vol. 7, no. 8, Aug. 2017, Art. no. e015746.

[8] J. Weller and A. Budson, "Current understanding of Alzheimer's disease diagnosis and treatment," *F1000Research*, vol. 7, 2018.

[9] B. Dubois, H. H. Feldman, C. Jacova, S. T. DeKosky, P. Barberger-Gateau, J. Cummings, A. Delacourte, D. Galasko, S. Gauthier, G. Jicha, K. Meguro, J. O'Brien, F. Pasquier, P. Robert, M. Rossor, S. Salloway, Y. Stern, P. J. Visser, and P. Scheltens, "Research criteria for the diagnosis of Alzheimer's disease: Revising the NINCDS–ADRDA criteria," *Lancet Neurol.*, vol. 6, no. 8, pp. 734–746, Aug. 2007.

[10] B. Dubois, A. Padovani, P. Scheltens, A. Rossi, and G. Dell'Agnello, "Timely diagnosis for Alzheimer's disease: A literature review on benefits and challenges," *J. Alzheimer's Disease*, vol. 49, no. 3, pp. 617–631, Dec. 2015.

[11] G. B. Frisoni, N. C. Fox, C. R. Jack, P. Scheltens, and P. M. Thompson, "The clinical use of structural MRI in Alzheimer disease," *Nature Rev. Neurol.*, vol. 6, no. 2, pp. 67–77, Feb. 2010. [Online]. Available: https://www.ncbi.nlm.nih.gov/pmc/articles/PMC2938772/

[12] F. Gao, "Integrated positron emission tomography/magnetic resonance imaging in clinical diagnosis of Alzheimer's disease," *Eur. J. Radiol.*, vol. 145, Dec. 2021, Art. no. 110017.

[13] P. L. McGeer, H. Kamo, R. Harrop, E. G. McGeer, W. R. W. Martin, B. D. Pate, and D. K. B. Li, "Comparison of PET, MRI, and CT with pathology in a proven case of Alzheimer's disease," *Neurology*, vol. 36, no. 12, p. 1569, Dec. 1986.

[14] X. Liu, K. Chen, T. Wu, D. Weidman, F. Lure, and J. Li, "Use of multimodality imaging and artificial intelligence for diagnosis and prognosis of early stages of Alzheimer's disease," *Transl. Res.*, vol. 194, pp. 56–67, Apr. 2018.

[15] P. Szolovits, R. S. Patil, and W. B. Schwartz, "Artificial intelligence in medical diagnosis," *Ann. Internal Med.*, vol. 108, no. 1, pp. 80–87, 1988.

[16] E. Neri, F. Coppola, V. Miele, C. Bibbolino, and R. Grassi, "Artificial intelligence: Who is responsible for the diagnosis?" *La Radiol. Medica*, vol. 125, no. 6, pp. 517–521, Jun. 2020.

[17] M. Tanveer, B. Richhariya, R. U. Khan, A. H. Rashid, P. Khanna, M. Prasad, and T. C. Lin, "Machine learning techniques for the diagnosis of Alzheimer's disease: A review," *ACM Trans. Multimedia Comput. Commun. Appl.*, vol. 16, no. 1, pp. 1–35, Apr. 2020.

[18] H. Bhasin and R. K. Agrawal, "A combination of 3-D discrete wavelet transform and 3-D local binary pattern for classification of mild cognitive impairment," *BMC Med. Informat. Decis. Making*, vol. 20, no. 1, pp. 1–10, Feb. 2020.

[19] W. S. Noble, "What is a support vector machine?" *Nature Biotechnol.*, vol. 24, no. 12, pp. 1565–1567, 2006.

[20] B. Magnin, L. Mesrob, S. Kinkingnéhun, M. Pélégrini-Issac, O. Colliot, M. Sarazin, B. Dubois, S. Lehéricy, and H. Benali, "Support vector machine-based classification of Alzheimer's disease from whole-brain anatomical MRI," *Neuroradiology*, vol. 51, no. 2, pp. 73–83, Feb. 2009.

[21] C. Salvatore, P. Battista, and I. Castiglioni, "Frontiers for the early diagnosis of AD by means of MRI brain imaging and support vector machines," *Current Alzheimer Res.*, vol. 13, no. 5, pp. 509–533, Mar. 2016.

[22] S. Liu, S. Liu, W. Cai, S. Pujol, R. Kikinis, and D. Feng, "Early diagnosis of Alzheimer's disease with deep learning," in *Proc. IEEE 11th Int. Symp. Biomed. Imag. (ISBI)*, Apr./May 2014, pp. 1015–1018.

[23] D. Anguita, A. Ghio, N. Greco, L. Oneto, and S. Ridella, "Model selection for support vector machines: Advantages and disadvantages of the machine learning theory," in *Proc. Int. Joint Conf. Neural Netw. (IJCNN)*, Jul. 2010, pp. 1–8.

[24] S. Karamizadeh, S. M. Abdullah, M. Halimi, J. Shayan, and M. J. Rajabi, "Advantage and drawback of support vector machine functionality," in *Proc. Int. Conf. Comput., Commun., Control Technol. (I4CT)*, Sep. 2014, pp. 63–65.

[25] C. Dumitru and V. Maria, "Advantages and disadvantages of using neural networks for predictions," *Ovidius Univ. Ann., Ser. Econ. Sci.*, vol. 13, no. 1, pp. 444–449, 2013.

[26] M. Kamal, A. R. Pratap, M. Naved, A. S. Zamani, P. Nancy, M. Ritonga, S. K. Shukla, and F. Sammy, "Machine learning and image processing enabled evolutionary framework for brain MRI analysis for Alzheimer's disease detection," *Comput. Intell. Neurosci.*, vol. 2022, pp. 1–8, Mar. 2022.

[27] Y. Wang, W. Zhou, C. Yu, and W. Su, "Assisted magnetic resonance imaging diagnosis for Alzheimer's disease based on kernel principal component analysis and supervised classification schemes," *J. Inf. Process. Syst.*, vol. 17, pp. 178–190, Feb. 2021.

[28] A. Farooq, S. Anwar, M. Awais, and S. Rehman, "A deep CNN based multi-class classification of Alzheimer's disease using MRI," in *Proc. IEEE Int. Conf. Imag. Syst. Techn. (IST)*, Oct. 2017, pp. 1–6.

[29] Y. Abdulazeem, W. M. Bahgat, and M. Badawy, "A CNN based framework for classification of Alzheimer's disease," *Neural Comput. Appl.*, vol. 33, no. 16, pp. 10415–10428, Aug. 2021.

[30] L. R. Medsker and L. C. Jain, "Recurrent neural networks," *Des. Appl.*, vol. 5, pp. 64–67, Dec. 2001.

[31] M. Riedmiller, "Advanced supervised learning in multi-layer perceptrons—From backpropagation to adaptive learning algorithms," *Comput. Standards Interfaces*, vol. 16, no. 3, pp. 265–278, Jul. 1994.

[32] D. AlSaeed and S. F. Omar, "Brain MRI analysis for Alzheimer's disease diagnosis using CNN-based feature extraction and machine learning," *Sensors*, vol. 22, no. 8, p. 2911, Apr. 2022.

[33] R. Hogan and C. Christoforou, "Alzheimer's detection through 3D convolutional neural networks," in *Proc. Int. FLAIRS Conf.*, Apr. 2021, vol. 34, no. 1, pp. 1–4.

[34] R. R. Janghel and Y. K. Rathore, "Deep convolution neural network based system for early diagnosis of Alzheimer's disease," *IRBM*, vol. 42, no. 4, pp. 258–267, Aug. 2021.

[35] S. Alinsaif and J. Lang, "3D shearlet-based descriptors combined with deep features for the classification of Alzheimer's disease based on MRI data," *Comput. Biol. Med.*, vol. 138, Nov. 2021, Art. no. 104879.

[36] R. Logan, B. G. Williams, M. F. da Silva, A. Indani, N. Schcolnicov, A. Ganguly, and S. J. Miller, "Deep convolutional neural networks with ensemble learning and generative adversarial networks for Alzheimer's disease image data classification," *Frontiers Aging Neurosci.*, vol. 13, p. 497, Aug. 2021.

[37] B. A. Mohammed, E. M. Senan, T. H. Rassem, N. M. Makbol, A. A. Alanazi, Z. G. Al-Mekhlafi, T. S. Almurayziq, and F. A. Ghaleb, "Multi-method analysis of medical records and MRI images for early diagnosis of dementia and Alzheimer's disease based on deep learning and hybrid methods," *Electronics*, vol. 10, no. 22, p. 2860, Nov. 2021.

[38] M. Anitha, V. Karpagam, and P. T. Selvy, "Diagnostic framework for automatic classification and visualization of Alzheimer's disease with feature extraction using wavelet transform," *NeuroQuantology*, vol. 19, no. 7, pp. 84–95, Aug. 2021.

[39] S. H. Subbaraya and S. S. Parthasarathy, "Probabilistic principal component analysis and long short-term memory classifier for automatic detection of Alzheimer's disease using MRI brain images," *Int. J. Knowl.-based Intell. Eng. Syst.*, vol. 26, no. 1, pp. 53–64, Jun. 2022.

[40] S. Urooj, S. P. Singh, A. Malibari, F. Alrowais, and S. Kalathil, "Early detection of Alzheimer's disease using polar harmonic transforms and optimized wavelet neural network," *Appl. Sci.*, vol. 11, no. 4, p. 1574, Feb. 2021.

[41] A. Sherin and R. Rajeswari, "Computer-aided diagnosis system for Alzheimer's disease using positron emission tomography images," *Interdiscipl. Sci., Comput. Life Sci.*, vol. 13, no. 3, pp. 433–442, Apr. 2021.

[42] S. Sulaiman and H. Abdullah, "Comparison study for three compression techniques (wavelet, contourlet and curvelet transformation)," *Al-Rafidain J. Comput. Sci. Math.*, vol. 15, no. 1, pp. 101–114, Jun. 2021.

[43] P. Görgel, "A brain tumor detection system using gradient based watershed marked active contours and curvelet transform," *Trans. Emerg. Telecommun. Technol.*, vol. 32, no. 9, Nov. 2020, Art. no. e4170.

[44] A. G. Tzalavra, I. Andreadis, K. Dalakleidi, F. Constantinidis, E. Zacharaki, and K. Nikita, "Dynamic contrast enhanced-magnetic resonance imaging radiomics combined with a hybrid adaptive neuro-fuzzy inference system-particle swarm optimization approach for breast tumour classification," *Expert Syst.*, vol. 39, no. 4, Dec. 2021, Art. no. e12895.

[45] T. Reddy and N. Kumaravel, "Segmentation and classification of jaw bone CT images using curvelet based texture features," *Bangladesh J. Med. Sci.*, vol. 9, no. 1, pp. 33–43, Jan. 1970.

[46] Y. Huang, F. Zhou, and J. Gilles, "Empirical curvelet based fully convolutional network for supervised texture image segmentation," *Neurocomputing*, vol. 349, pp. 31–43, Jul. 2019.

[47] T. Yun, Y. Q. Xu, and L. Cao, "Semi-supervised ultrasound image segmentation based on curvelet features," *Appl. Mech. Mater.*, vols. 239–240, pp. 104–114, Dec. 2012.

[48] O. Dehzangi and M. Taherisadr, "Human gait identification using two dimensional multi-resolution analysis," *Smart Health*, vol. 19, Mar. 2021, Art. no. 100167.

[49] A. Deka, "Offline handwritten signature verification using distance based classifier," *Int. J. Adv. Sci. Res. Manage.*, vol. 4, no. 8, pp. 1–4, Aug. 2019.

[50] A. Haitham Najim and A. Majeed Ali, "Face recognition using various feature extraction approaches," *IOP Conf. Ser., Mater. Sci. Eng.*, vol. 928, no. 3, Nov. 2020, Art. no. 032060.

[51] S. Biswas and J. Sil, "An efficient face recognition method using contourlet and curvelet transform," *J. King Saud Univ., Comput. Inf. Sci.*, vol. 32, no. 6, pp. 718–729, Jul. 2020.

[52] P. Singh and N. Dodke, "Facial expression recognition from visual information using curvelet transform," *Int. J. Comput. Appl.*, vol. 134, no. 10, pp. 30–33, Jan. 2016.

[53] T. Wiem and D. Ali, "Deep convolutional second generation curvelet transform-based MR image for early detection of Alzheimer's disease," in *Proc. 16th Int. Joint Conf. Comput. Vis., Imag. Comput. Graph. Theory Appl.*, 2021, pp. 285–292.

[54] D. Jha and G.-R. Kwon, "Alzheimer disease detection in MRI using curvelet transform with K-NN," *J. Korean Inst. Inf. Technol.*, vol. 14, no. 8, p. 121, Aug. 2016.

[55] E. Candès, L. Demanet, D. Donoho, and X. Ying, "Fast discrete curvelet transforms," *Multiscale Model. Simul.*, vol. 5, no. 3, pp. 861–899, Sep. 2006.

[56] G. Tang and J. Ma, "Application of total-variation-based curvelet shrinkage for three-dimensional seismic data denoising," *IEEE Geosci. Remote Sens. Lett.*, vol. 8, no. 1, pp. 103–107, Jan. 2011.

[57] C. Zhang, H.-B. Lin, Y. Li, and B.-J. Yang, "Seismic random noise attenuation by time-frequency peak filtering based on joint time-frequency distribution," *Comp. Rendus Geosci.*, vol. 345, nos. 9–10, pp. 383–391, Sep. 2013.

[58] D. L. Donoho and J. M. Johnstone, "Ideal spatial adaptation by wavelet shrinkage," *Biometrika*, vol. 81, no. 3, pp. 425–455, Sep. 1994.

[59] H. Lin, Y. Li, C. Zhang, and H. Ma, "Curvelet domain denoising based on kurtosis characteristics," *J. Geophys. Eng.*, vol. 12, no. 3, pp. 419–426, May 2015.

[60] E. Mggdadi, A. Al-Aiad, M. S. Al-Ayyad, and A. Darabseh, "Prediction Alzheimer's disease from MRI images using deep learning," in *Proc. 12th Int. Conf. Inf. Commun. Syst. (ICICS)*, May 2021, pp. 120–125.

[61] K. U. Rani, S. S. Sharvari, M. G. Umesh, and B. C. Vinay, "Binary classification of Alzheimer's disease using MRI images and support vector machine," in *Proc. IEEE Mysore Sub Sect. Int. Conf. (MysuruCon)*, Oct. 2021, pp. 423–426.

[62] E. Kaplan, S. Dogan, T. Tuncer, M. Baygin, and E. Altunisik, "Feed-forward LPQNet based automatic Alzheimer's disease detection model," *Comput. Biol. Med.*, vol. 137, Oct. 2021, Art. no. 104828.

[63] S. Sharma, S. Gupta, D. Gupta, A. Altameem, A. K. J. Saudagar, R. C. Poonia, and S. R. Nayak, "HTLML: Hybrid AI based model for detection of Alzheimer's disease," *Diagnostics*, vol. 12, no. 8, p. 1833, Jul. 2022.

[64] M. H. Al-Adhaileh, "Diagnosis and classification of Alzheimer's disease by using a convolution neural network algorithm," *Soft Comput.*, vol. 26, pp. 7751–7762, Jan. 2022.

[65] S. Murugan, C. Venkatesan, M. G. Sumithra, X.-Z. Gao, B. Elakkiya, M. Akila, and S. Manoharan, "DEMNET: A deep learning model for early diagnosis of Alzheimer diseases and dementia from MR images," *IEEE Access*, vol. 9, pp. 90319–90329, 2021.

CHAHD M. CHABIB was born in Abu Dhabi, United Arab Emirates, in January 1998. She received the B.Sc. degree in chemical engineering from Khalifa University, Abu Dhabi, in 2020. Since 2020, she has been a Research Assistant with the Department of Biomedical Engineering, Khalifa University. Her current research interests include data analysis, image processing, and computer vision.

LEONTIOS J. HADJILEONTIADIS (Senior Member, IEEE) was born in Kastoria, Greece, in 1966. He received the first Diploma degree in electrical engineering and the first Ph.D. degree in electrical and computer engineering from the Aristotle University of Thessaloniki (AUTH), Thessaloniki, Greece, in 1989 and 1997, respectively, the second Ph.D. degree in music composition from the University of York, York, U.K., in 2004, and the second Diploma degree in musicology from AUTH, in 2011. He has published over 100 articles in peer-reviewed international journals, over 150 papers in peer-reviewed international conference proceedings, six books, two books edited, 24 book chapters, and three patents [H-index is 37 (Google scholar) and 28 (Scopus)]. Currently, he is the Coordinator/Scientific Responsible for three EU FP7/H2020 projects with a total budget of up to EUR ten Million. He was awarded as an Innovative Researcher and the Champion Faculty from Microsoft, USA, in 2012. He also has strong collaborations with international research networks/centers (e.g., Karolinska Institutet, Fraunhofer Institute, Kings College London, Harvard/MIT, and Winnipeg University). His research interests include advanced signal processing, machine learning, biomedical engineering, affective computing, and active and healthy ageing. He is a member of the Technical Chamber of Greece, the Higher-Order Statistics Society, the International Lung Sounds Association, the American College of Chest Physicians, and the Greek Composers' Union (Vice-President).

AAMNA AL SHEHHI received the bachelor's degree in software engineering from United Arab Emirates University, Abu Dhabi, United Arab Emirates, in 2009, and the master's degree in computing and information science and the Ph.D. degree in interdisciplinary engineering from the Masdar Institute of Science and Technology, Abu Dhabi, in collaboration with the Massachusetts Institute of Technology (MIT), in 2013 and 2017, respectively. During her Ph.D., she was a part of an exchange program for one semester with MIT, in 2015. During her studies, her research was based on time series analysis, big data analysis, and machine learning modeling for weather forecasting for different weather stations in United Arab Emirates and Twitter data analysis in the context of the Arab world with a special focus on United Arab Emirates. This involved a combination of sentiment analysis, complex collective behavior, and natural language processing. In 2017, she joined Khalifa University, Abu Dhabi, United Arab Emirates, and MIT as a Postdoctoral Fellow. She also joined Imperial College London, as an Honorary Research Associate with the School of Public Health, Epidemiology and Biostatistics Inc., MRC-PHE Centre. Currently, she is an Assistant Professor with the Department of Biomedical Engineering, Khalifa University. Her research interests include causal inference, machine learning, and artificial intelligence for the medical domain.